Cytometry
PART A
Journal of the International Society for Advancement of Cytometry

Study of Low Speed Flow Cytometry for Diffraction Imaging with Different Chamber and Nozzle Designs

Yu Sa,[1] Yuanming Feng,[1,2*] Kenneth M. Jacobs,[2] Jun Yang,[1] Ran Pan,[1] Ioannis Gkigkitzis,[2] Jun Q. Lu,[2] Xin-Hua Hu[1,2*]

[1]Department of Biomedical Engineering, Tianjin University, Tianjin 300072, China

[2]Department of Physics, East Carolina University, Greenville, North Carolina 27858

Received 24 January 2013; Revised 31 May 2013; Accepted 7 June 2013

Grant sponsor: North Carolina Biotechnology Center; Grant number: 2010-TEG-1501; Grant sponsor: Golfers Against Cancer; Grant number: 2012-13-GAC; Grant sponsor: National Science Foundation of China; Grant numbers: 81041107, 81171342.

Additional Supporting Information may be found in the online version of this article.

Correspondence to: Xin-Hua Hu, Department of Physics, East Carolina University, Greenville, NC 27858, USA. E-mail: hux@ecu.edu and Yuanming Feng, Department of Biomedical Engineering, Tianjin University, Tianjin 300072, China. E-mail: ymfeng@tju.edu.cn

Published online 9 July 2013 in Wiley Online Library (wileyonlinelibrary.com)

DOI: 10.1002/cyto.a.22332

Abstract

Achieving effective hydrodynamic focusing and flow stability at low speed presents a challenging design task in flow cytometry for studying phenomena such as cell adhesion and diffraction imaging of cells with low-cost cameras. We have developed different designs of flow chamber and sheath nozzle to accomplish the above goal. A 3D computational model of the chambers has been established to simulate the fluid dynamics in different chamber designs and measurements have been performed to determine the velocity and size distributions of the core fluid from the nozzle. Comparison of the simulation data with experimental results shows good agreement. With the computational model significant insights were gained for optimization of the chamber design and improvement of the cell positioning accuracy for study of slow moving cells. The benefit of low flow speed has been demonstrated also by reduced blurring in the diffraction images of single cells. Based on these results, we concluded that the new designs of chamber and sheath nozzle produce stable hydrodynamic focusing of the core fluid at low speed and allow detailed study of cellular morphology under various rheological conditions using the diffraction imaging method. © 2013 International Society for Advancement of Cytometry

Key terms

flow cytometry; hydrodynamic focusing; chamber design; diffraction imaging

FLOW cytometry (FCM) produces a laminar flow consisting of the sheath and core fluids to transport and accurately position the cells or particles, carried by the core fluid, in single file through one or more light beams for interrogation. Current flow chamber designs typically utilize a sheath nozzle with a conical end or orifice for hydrodynamic focusing the fluid injected by the core nozzle to produce a fast moving laminar flow for high throughput assay of cells optically (1–4). The high flow speeds usually range from 1 to 10 m/s in an FCM instrument and yield rheological conditions quite different from those in blood vessels, in which cells often move at speeds less or much less than 10 mm/s (5). To study slow moving cells or investigate phenomena such as cell adhesion (6–9), for example, it is highly desired and necessary to achieve hydrodynamic focusing of the core fluid at low speed that also reduce significantly the speed gradient experienced by the moving cells (3). Several designs of flow chamber have been reported to move cells or organelles at low speeds near 10 mm/s using small-bore capillary tubes or flow chambers of narrow channel using hydrodynamic (10,11) or acoustic focusing (12). But these designs introduce glass-water interfaces very close to the cells or particles to be interrogated optically with narrow tubes or channels or increased system complexity with acoustic focusing. The interfaces usually give rise to strong background scatters coexisting with the scatters from the targeted particles at the same wavelength because of the large mismatch of refractive index between glass and water. This problem alone prevents the applica-

tions of these designs in imaging FCM, especially in the case of imaging coherent light scatters from the target particles at the same wavelength of excitation. Accordingly, one has to meet the challenge of producing clinically relevant flow conditions with hydrodynamic focusing implemented in index-matched medium at low speed.

Existing FCM methods have two limitations. First, they provide inadequate morphological information about cells. Secondly, the reliance on fluorescence signals as the major source of information for cellular assay requires cell staining, which is expensive, labor intensive and time consuming. Imaging FCM instruments now are available for acquiring noncoherent fluorescent and dark/bright field microscopy images (13,14). Still the limitation of staining requirement remains and automated extraction of morphological information from noncoherent images is very difficult, if not impossible, with presently available algorithms for the need of segmentation. Therefore, these images have to be stored for off-line analysis under human supervision. Furthermore, the noncoherent images present 2D projections of 3D morphology of the imaged cells with the third dimension compressed. It is well known that coherently scattered wavefields, x-ray or optical, can be measured as diffraction images to determine 3D morphology of the scattering particle (15,16). Over the past decade, the feasibility to acquire diffraction images from moving particles has been demonstrated with various devices (17–19). But the 3D reconstruction requires acquisition of numerous diffraction images and intensive computing and is obviously impractical for implementation into the FCM platform.

Through experimental and numerical investigations, we have shown that the texture features of diffraction images acquired with FCM can be rapidly extracted with existing image processing algorithms for automated assay and classification of the imaged particles including biological cells (20–23). Different from noncoherent images, diffraction images present speckle patterns with no need to segment and can be processed automatically in real time to extract parameters as the "fingerprint" features of the imaged particle's 3D morphology for analysis. We have termed this new approach of coherent image acquisition and analysis as the diffraction imaging flow cytometry (DIFC) method. Acquisition of high-contrast diffraction images is critical for the DIFC method to extract accurate image features for cellular assay. It is thus important to reduce the strong background noise due to the light scattered from the index-mismatched interfaces outside the cell of interest. A fluidic design to transport cells through the incident laser beam at speeds below 10 mm/s is preferred for accumulating enough photons on low-cost cameras with negligible blurring. To achieve hydrodynamic focusing at low speed, we have studied various novel designs of the flow chamber and nozzle. Here we report results of computational and experimental investigations of the hydrodynamic focusing in flow chambers with different sheath nozzles for high-contrast diffraction imaging of cells and particles moving at flow speeds less than 10 mm/s. Results of diffraction images acquired from Jurkat cells at different flow speeds are also presented to demonstrate the benefits of low speed in reducing image blurring with the flow chamber.

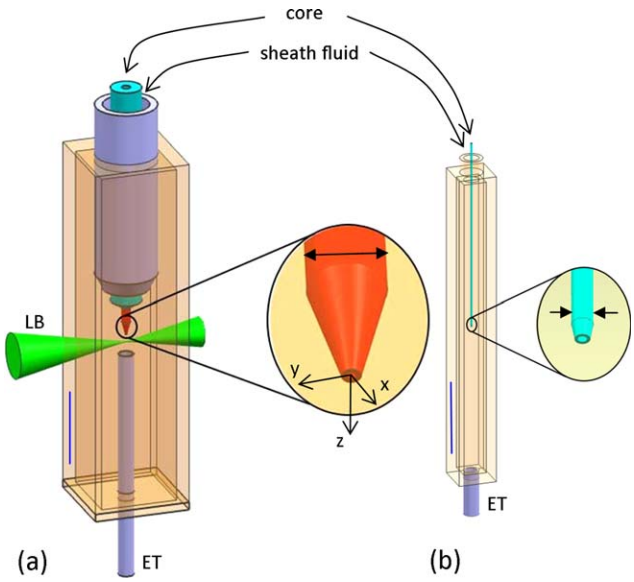

Figure 1. Schematics of two flow chambers with straight sheath nozzle: (**a**) a large chamber of $w = 10$ mm and $L = 45$ mm, bar: 10 mm, enlarged view: OD (arrow line) = 1.20 mm; (**b**) a small chamber of $w = 3$ mm and $L = 40$ mm, bar: 10 mm, enlarged view: OD = 0.24 mm. LB, incident laser beam; ET, exit tube. [Color figure can be viewed in the online issue which is available at wileyonlinelibrary.com.]

Materials and Methods

Hydrodynamic focusing with a sheath fluid forms a laminar flow for stable positioning of cells at the focus of an incident laser beam. For high-contrast diffraction imaging of the single flowing cells, it is vitally important to decrease the image noise by light scattered at the refractive-index-mismatched interface such as the sheath fluid and chamber wall. This requirement necessitates the use of a large sized index-matched medium between the sheath fluid and chamber wall of glass. A "jet-in-fluid" design has been developed for our DIFC system to inject the laminar flow from two nozzles into a host fluid, of the same refractive index as that of sheath, inside a flow chamber (20). Different from conventional designs of a sheath nozzle with orifice (1–4), we have experimentally studied and developed various nozzle designs without conical orifice for injecting the sheath fluid into a water-filled flow chamber to produce desired hydrodynamic focusing at low speed (20,23). To optimize these designs efficiently, computational models of different flow chambers were constructed and investigated with two examples presented in Figure 1. In the large chamber shown in Figure 1a, a stainless tube of inside diameter of $ID_s = 6$ mm functions as the sheath nozzle to hydrodynamically focus the core fluid out of a ceramic nozzle of $ID_c = 125$ μm in a large glass chamber of $w = 10$ mm and $L = 45$ mm, where w is the side length of the square transvers cross-section and L is the length. By comparison, Figure 1b displays a small flow chamber of $w = 3$ mm

and $L = 40$ mm. Two concentric tubes of $ID_s = 2$ mm and $ID_c = 110$ μm inject the sheath and core fluid into the chamber. In either design an exit tube sinks the injected fluids out of the chamber.

For numerical simulations of the fluid velocity $\boldsymbol{u} = (u_1, u_2, u_3)$ in each of the two flow chambers, the Navier–Stokes equations are solved for water as the medium of the fluid which is treated as a Newtonian and incompressible viscous fluid together with the equation of continuity using the Multiphysics software (version 4.2, COMSOL, Burlington, MA USA). For a fluid of constant mass density ρ, the two equations can be written as

$$\rho\left(\frac{\partial \mathbf{u}}{\partial t} + (\mathbf{u}\cdot\nabla)\mathbf{u}\right) = -\nabla p + \rho\mathbf{g} + \mu\nabla^2\mathbf{u} \quad (1)$$

$$\nabla\cdot\mathbf{u} = 0 \quad (2)$$

where p is the fluid pressure, g is the gravity acceleration, and μ is the dynamic viscosity. The boundary conditions consist of the flow rates F_s and F_c of the sheath and core fluids, respectively, a no-slip condition at the fluid boundary with the chamber walls and a constant pressure of 1.00 atm at the exit tube. Since the cross sections of the flow chambers are not axial symmetric, the 3D modeling option of the Multiphysics software was called with a user controlled tetrahedral mesh of variable sizes from 0.002 to 0.670 mm. In addition to the simulation of velocity $\boldsymbol{u}(\boldsymbol{r})$, we have also employed the streamline option to identify the core fluid in the laminar flow for determination of its diameter $d_c(z)$ at different locations, where z is the vertical distance from the end of the core nozzle in the flow chamber.

A DIFC experimental system with a split-view imaging unit was constructed to accurately control the flow rates of the sheath and core fluids using two in-house built syringe pumps driven by precision servo DC motors. The imaging unit consists a microscope objective (M Plan Apo 50x, Mitutoyo Aurora, IL USA), a beam spliter, tube lenses and two cameras as described in details previously (21,23). The objective collects either coherent light scattered from single cells excited by a laser beam focused on the core fluid for diffraction imaging or incoherent light from the laminar flow with the chamber illuminated by a white light source for alignment and flow measurement. The imaging unit was placed in a focusing position for measurement of speed and diameter of the core flow under the incoherent illumination of white light. At this position the images at the camera sensors conjugate with the tip of the core nozzle or core fluid. Diffraction imaging was achieved by translating the imaging unit off the focusing position toward the flow chamber in a range from 50 to 300 μm.

Results

By setting the first term on the left hand side of Eq. (1) to zero, we simulated the steady-state distributions of fluid velocity $\boldsymbol{u}(\boldsymbol{r})$ by using the Multiphysics software to solve Eqs. (1) and (2) with the boundary conditions discussed above.

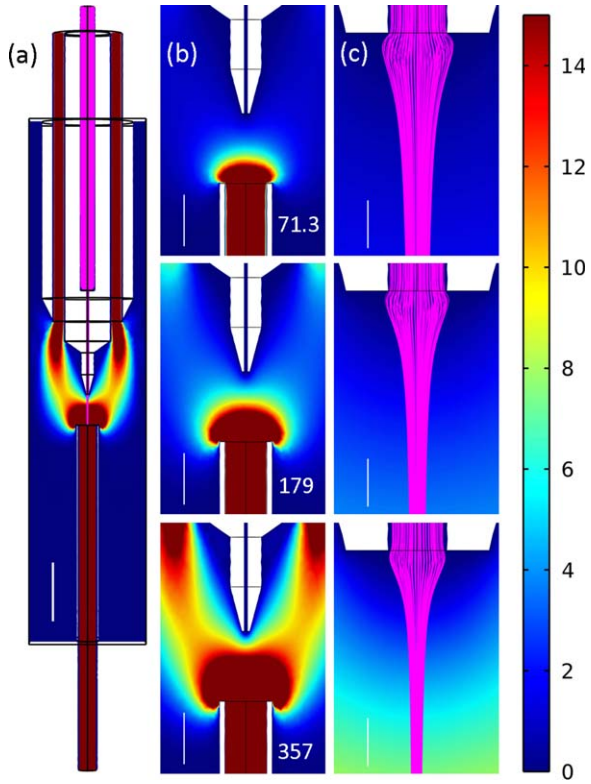

Figure 2. Cross-sectional views of simulated flow speed distribution and streamlines (pink colored) in the large flow chamber of $w = 10$ mm outside the tubes and core nozzle: (**a**) within the chamber body with the sheath fluid flow rate $F_s = 357$ μL/s; (**b**) between the core nozzle and exit tube at different values of F_s in (μL/s) as marked; (**c**) near the core nozzle at the same set of F_s as those in (b). Bars: (a) 5.00 mm; (b) 2.00 mm; (c) 0.10 mm. All results were obtained with the core fluid flow rate $F_c = 0.0035$ μL/s and speed values are in the unit of mm/s. [Color figure can be viewed in the online issue which is available at wileyonlinelibrary.com.]

More details of the simulation procedures are provided in the Supporting Information. For the large flow chamber of $w = 10$ mm shown in Figure 1a, the false-color presentations of flow speed, $u(\boldsymbol{r}) = |\boldsymbol{u}(\boldsymbol{r})|$, and streamline presentations of the velocity direction for the core fluid are displayed in Figure 2 on different scales. The pink-colored streamlines for the core fluid in Figures 2a and 2c and $u(\boldsymbol{r})$ in Figure 2b illustrate clearly that a sheath nozzle made of straight tube has the capacity for hydrodynamic focusing in the flow chamber at speeds lower than 10 mm/s by forcing the sheath fluid into the exit tube. This new design feature is beneficial not only in production of a large space of clear fluid with index matching to the sheath for high-contrast imaging of the flowing cells but also in significant simplification of nozzle construction. Figure 2b exhibits additional details in magnified views of $u(\boldsymbol{r})$ between the tip of the core nozzle and the exit tube at three different values of sheath flow rate F_s and Figure 2c presents further magnified views for speed distribution of the sheath fluid near the tip of core nozzle and the streamlines of the core fluid. By comparing the three cases in Figures 2b and 2c

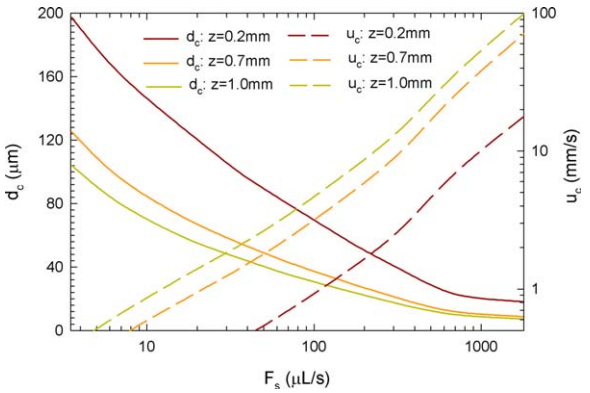

Figure 3. The simulated dependence of the core fluid diameter d_c and speed u_c on sheath flow rate F_s at different distance z from the tip of the core nozzle and a fixed core flow rate of $F_c = 0.0035$ μL/s. [Color figure can be viewed in the online issue which is available at wileyonlinelibrary.com.]

for different sheath flow rates F_s one can see that the core fluid's speed u_c and diameter d_c at different distances from the core nozzle tip can be varied by adjusting F_s. Figure 3 plots the simulated results of the core speed u_c and diameter d_c of the core fluid versus the sheath flow rate F_s with a fixed core flow rate F_c. Measured images are presented in Figure 4 with three diffraction images of single microspheres and cell acquired at the mid-point between the tip of core nozzle and the exit tube in this flow chamber and one noncoherent image of the focused core fluid as it leaves the core nozzle. The two dark spots in the lower portion of Figure 4d are particles attached to the chamber wall. Compared to the diffraction images published previously (17–19), the contrasts of these diffraction images are markedly improved with the water-filled flow chamber.

The simulation data presented in Figures 2–4 confirm our experimental observations that the new design of sheath nozzle allows excellent focusing of the core fluid at low speed for acquisition of high-contrast diffraction images (20,23). Flow chambers of large w, however, exhibited high sensitivity of cell positioning to external vibration in our DIFC measurements. To improve the flow stability, we have investigated chamber designs with reduced transverse dimensions with an optimized configuration of chamber and nozzles illustrated in Figure 1b. Numerical simulations have been performed on this new configuration with the results of flow speed distribution $u(\boldsymbol{r})$ and core streamlines presented in Figure 5. We have also performed measurements of $u_c(z)$ and $d_c(z)$ of the core fluid made of 10% mixture of glycerol in water for visualizing its interface with the sheath fluid of water. The mismatch of refractive index between the core and sheath fluids permits determination of d_c under illumination by a noncoherent white light source, as demonstrated in Figure 4d. The core fluid speed u_c was measured from the length of blurred track of microspheres on the image taken by the camera using

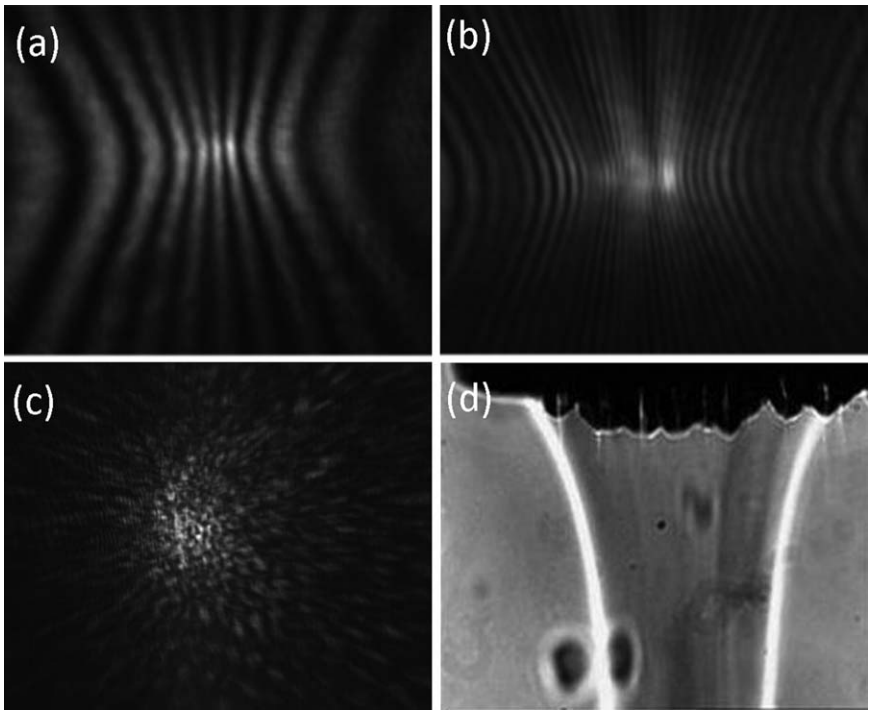

Figure 4. Diffraction images of (**a**) one polystyrene microsphere of diameter $D = 9.6$ μm; (**b**) one microsphere of $D = 25$ μm; (**c**) one MCF-7 breast cancer cell; and (**d**) a noncoherent image of the hydrodynamically focused core fluid (mixture of 10% glycerol in water) by the sheath fluid of water outside of the core nozzle tip under a white light illumination. The images of (a) to (c) were acquired under the excitation of an incident laser beam of 532 nm in wavelength and exposure time of 0.5 ms with core flow speed u_c about 10 mm/s at the laser beam focus. The off-focus translation distance is 150 μm toward the flow chamber for the imaging unit.

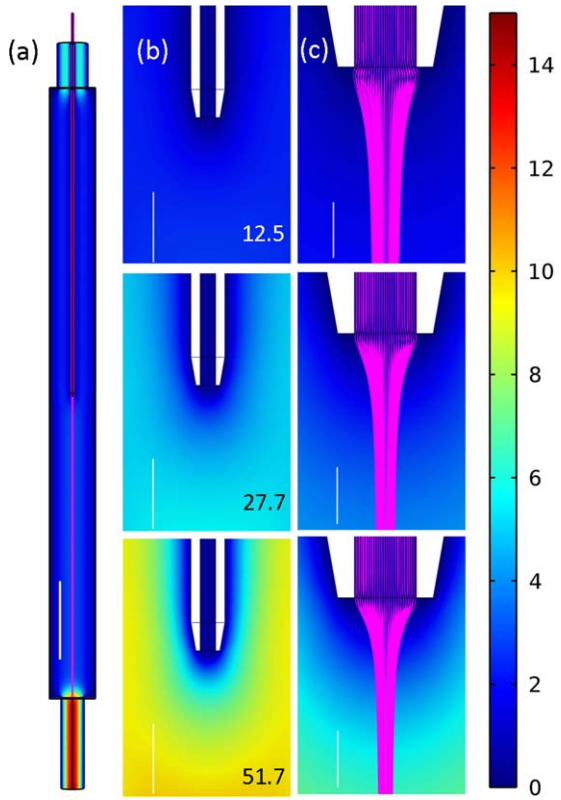

Figure 5. Cross-sectional views of simulated flow speed distribution and streamlines (pink colored) in the small flow chamber of $w = 3$ mm outside the tubes and core nozzle: (**a**) within the chamber body with the sheath fluid flow rate $F_s = 12.5$ μL/s; (**b**) between the core nozzle and exit tube at different values of F_s in (μL/s) as marked; (**c**) near the core nozzle at the same set of F_s as those in (b). Bars: (a) 5.00 mm; (b) 0.50 mm; (c) 0.10 mm. All results were obtained with the core fluid flow rate $F_c = 0.0035$ μL/s and speed values are in the unit of mm/s. [Color figure can be viewed in the online issue which is available at wileyonlinelibrary.com.]

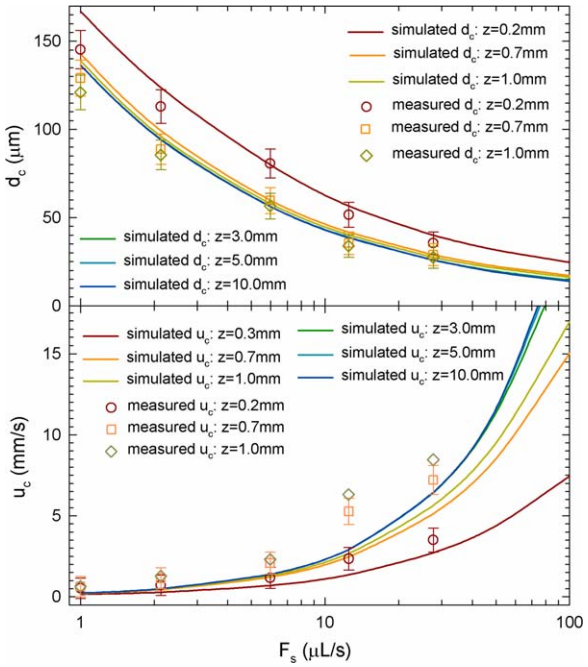

Figure 6. The simulated (lines) and measured (symbols) values of the core fluid diameter d_c and speed u_c versus sheath flow rate F_s at various distances z from the tip of the core nozzle and a fixed core flow rate of $F_c = 0.0035$ μL/s. [Color figure can be viewed in the online issue which is available at wileyonlinelibrary.com.]

extended exposure time around 10 ms under the same white light illumination. The simulated and measured results of $u_c(z)$ and $d_c(z)$ are presented in Figure 6, in which additional simulation data were obtained for $z > 0.7$ mm to examine the effect of hydrodynamic focusing with the new chamber design. To demonstrate the benefits of diffraction imaging at low speed, we have acquired diffraction images from cultured Jurkat cells, a T-lymphocyte leukaemia line, at different core fluid speeds of u_c =3 and 9 mm/s with examples shown in Figure 7.

Discussion

Hydrodynamic focusing of the core fluid by a sheath fluid is critically important to accurately position cells carried by the core through the laser beam focus in single file for FCM study. Fluidic designs using sheath nozzles with orifice have been well studied and widely applied for high speed transportation of the cells to achieve high throughput in FCM instrumentation. On the other hand, accomplishing accurate cell positioning at low speed is a challenging task but highly desired for investigation of cell adhesion and tethering under circulating conditions similar to those of human blood, which has attracted intense research interests for their effects on pathogenesis and treatment of diseases (6–9), in addition to the benefit of diffraction imaging with low-cost cameras as demonstrated by the results presented in Figure 4. After experimental investigations of various design concepts, we have developed flow chambers with straight sheath nozzles to produce desired hydrodynamic focusing of the core fluid at low speed. The computational model and fluid dynamic simulation data presented in this report yield strong evidence in support of our experimental finding and insight for further optimization of the chamber designs. Figures 3 and 6 show quantitatively the existence of a region for the sheath flow rate F_s in which the hydrodynamic focusing in terms of reducing d_c depends sensitively on F_s and size of flow chambers. For the larger chamber of $w = 10$ mm d_c drops markedly as F_s increases from 1 to about 500 μL/s while for the small chamber of $w = 3$ mm the similar drop in d_c occurs between 1 and about 50 μL/s. These simulation data agree fairly well with the measured values of d_c plotted in Figure 6 and our observations on the variation of F_s using different chambers. Furthermore, the small chamber with the exit tube placed at the bottom was observed to exhibit very long section of hydrodynamically focused core fluid from the tip of core nozzle. The experimental observation is supported by the additional simulation data in Figure 6, which shows nearly constant diameter d_c and speed u_c for z ranging from 1 to 10 mm. Within this section of well-collimated core fluid, we can vary the fluid speed to

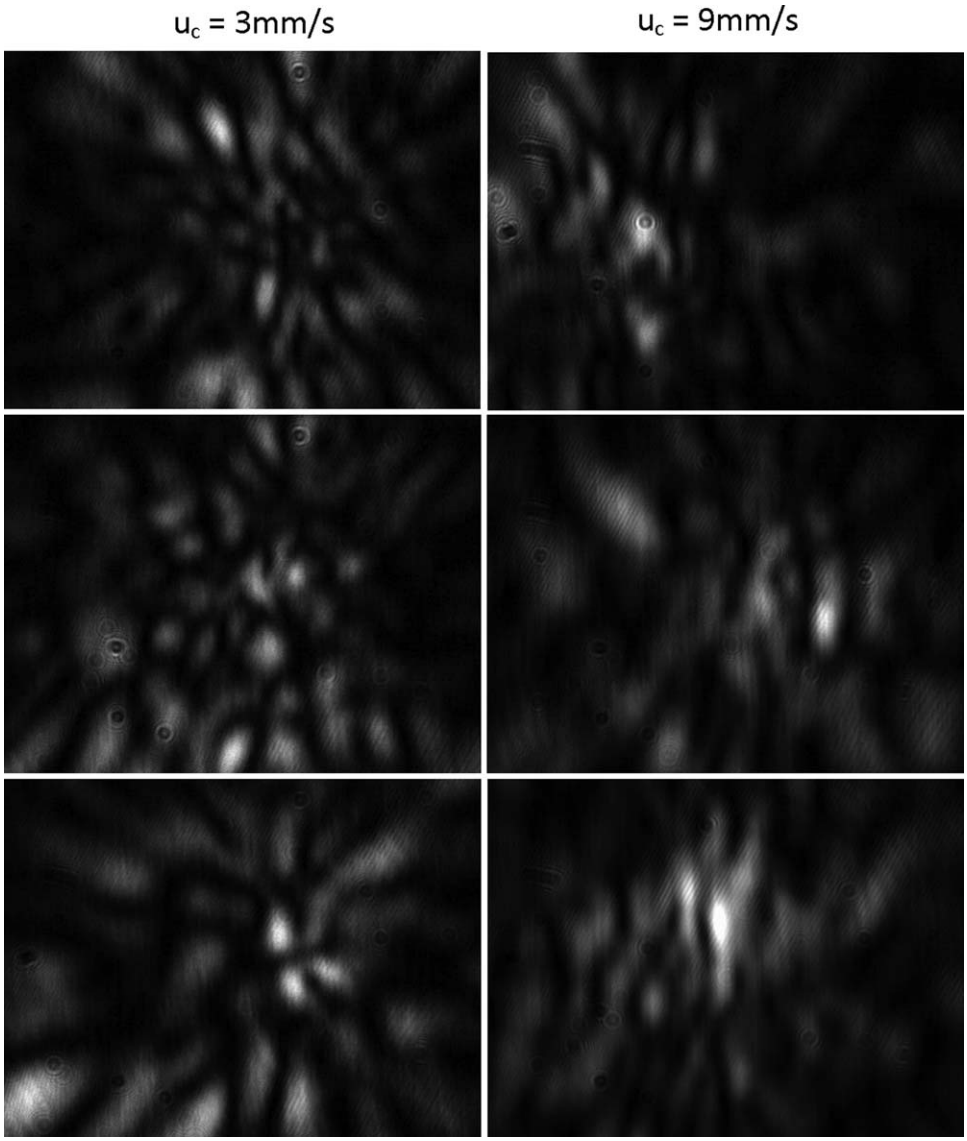

Figure 7. Diffraction images of single Jurkat cells at different core speed u_c with an exposure time of 1.0 ms: Left panel: $u_c = 3$ mm/s; right panel: $u_c = 9$ mm/s. Other conditions are the same as those in Fig. 4.

show that low speed can indeed reduce the blurring of the fringes in the diffraction images as presented by the examples in Figure 7 using a low-cost camera of 12-bit pixel depth (LU75M, Lumenera, Ottawa, Ontario, Canada). Together these results show clearly that the novel designs of flow chamber and sheath nozzles allow accurate positioning of cells or particles at low and clinically relevant speeds to investigate their morphology and rheology with the DIFC method.

Acknowledgments

The authors wish to thank Profs. Li V. Yang and Mary A. Farwell for providing the Jurkat and MCF-7 cells.

Literature Cited

1. Dean PN, Pinkel D, Mendelsohn ML. Hydrodynamic orientation of sperm heads for flow cytometry. Biophys J 1978;23:7–13.
2. Stovel RT, Sweet RG, Herzenberg LA. A means for orienting flat cells in flow systems. Biophys J 1978;23:1–5.
3. Amblard F, Cantin C, Durand J, Fischer A, Sékaly R, Auffray C. New chamber for flow cytometric analysis over an extended range of stream velocity and application to cell adhesion measurements. Cytometry 1992; 13:15–22.
4. Rens W, Welch GR, Johnson LA. A novel nozzle for more efficient sperm orientation to improve sorting efficiency of X and Y chromosome-bearing sperm. Cytometry 1998;33:476–481.
5. Gaehtgens P, Meiselman H, Wayland H. Velocity profiles of human blood at normal and reduced hematocrit in glass tubes up to 130 μ diameter. Microvasc Res 1970;2: 13–23.
6. Panés J, Perry M, Granger DN. Leukocyte-endothelial cell adhesion: Avenues for therapeutic intervention. Br J Pharmacol 1999;126:537–550.
7. Chang K-C, Tees DFJ, Hammer DA. The state diagram for cell adhesion under flow: Leukocyte rolling and firm adhesion. Proc Natl Acad Sci USA 2000;97:11262–11267.
8. Schwarz US, Alon R. L-selectin-mediated leukocyte tethering in shear flow is controlled by multiple contacts and cytoskeletal anchorage facilitating fast rebinding events. Proc Natl Acad Sci USA 2004;101:6940–6945.
9. Beste MT, Hammer DA. Selectin catch-slip kinetics encode shear threshold adhesive behavior of rolling leukocytes. Proc Natl Acad Sci USA 2008;105:20716–20721.

10. Wietzorrek J, Plesnila N, Baethmann A, Kachel V. A new multiparameter flow cytometer: Optical and electrical cell analysis in combination with video microscopy in flow. Cytometry 1999;35:291–301.
11. Habbersett RC, Jett JH. An analytical system based on a compact flow cytometer for DNA fragment sizing and single-molecule detection. Cytometry Part A 2004;60:125–134.
12. Goddard G, Martin JC, Graves SW, Kaduchak G. Ultrasonic particle-concentration for sheathless focusing of particles for analysis in a flow cytometer. Cytometry Part A 2006;69:66–74.
13. Ong SH, Horne D, Yeung CK, Nickolls P, Cole T. Development of an imaging flow cytometer. Anal Quant Cytol Histol 1987;9:375–382.
14. George TC, Basiji DA, Hall BE, Lynch DH, Ortyn WE, Perry DJ, Seo MJ, Zimmerman CA, Morrissey PJ. Distinguishing modes of cell death using the ImageStream multispectral imaging flow cytometer. Cytometry A 2004;59: 237–245.
15. Wedberg TC, Stamnes JJ. Recent results in optical diffraction microtomography. Meas Sci Technol 1996;4:414–418.
16. Shapiro D, Thibault P, Beetz T, Elser V, Howells M, Jacobsen C, Kirz J, Lima E, Miao H, Neiman AM, et al. Biological imaging by soft X-ray diffraction microscopy. Proc Natl Acad Sci USA 2005;102:15343–15346.
17. Holler S, Pan Y, Chang RK, Bottiger JR, Hill SC, Hillis DB. Two-dimensional angular optical scattering for the characterization of airborne microparticles. Opt Lett 1998; 23:1489–1491.
18. Neukammer J, Gohlke C, Hope A, Wessel T, Rinneberg H. Angular distribution of light scattered by single biological cells and oriented particle agglomerates. Appl Opt 2003;42:6388–6397.
19. Su XT, Singh K, Capjack C, Petracek J, Backhouse C, Rozmus W. Measurements of light scattering in an integrated microfluidic waveguide cytometer. J Biomed Opt 2008;13:024024.
20. Jacobs KM, Lu JQ, Hu XH. Development of a diffraction imaging flow cytometer. Opt Lett 2009;34:2985–2987.
21. Jacobs KM, Yang LV, Ding J, Ekpenyong AE, Castellone R, Lu JQ, Hu XH. Diffraction imaging of spheres and melanoma cells with a microscope objective. J Biophoton 2009;2:521–527.
22. Dong K, Feng Y, Jacobs KM, Lu JQ, Brock RS, Yang LV, Bertrand FE, Farwell MA, Hu XH. Label-free classification of cultured cells through diffraction imaging. Biomed Opt Express 2011;2:1717–1726.
23. Sa Y, Zhang J, Moran MS, Lu JQ, Feng Y, Hu XH. A novel method of diffraction imaging flow cytometry for sizing microspheres. Opt Express 2012;20: 22245–22251.